Journal of
Composites Science

MDPI

Article

Insulation Strategies to Enhance Fire Resistance in Composite Slabs with Reduced Carbon Emissions

Otavio G. N. Ribeiro [1], Paulo A. G. Piloto [2,*] and Gustavo de M. S. Gidrão [1]

[1] Campus de Guarapuava, Universidade Tecnológica Federal do Paraná (Federal University of Technology), Avenida Guarapuava, 800, Guarapuava 85053-525, Brazil; otavioribeiro@alunos.utfpr.edu.br (O.G.N.R.); gidrao@utfpr.edu.br (G.d.M.S.G.)
[2] GICoS, Instituto Politécnico de Bragança, Campus Santa Apolónia, 5300-253 Bragança, Portugal
* Correspondence: ppiloto@ipb.pt

Abstract

Composite slabs have gained popularity in modern high-rise construction due to their superior load-bearing capacity and reduced self-weight. The vulnerability of the unprotected steel deck under fire conditions poses serious challenges, as the rapid reduction in steel strength and stiffness can compromise structural resistance and accelerate fire spread. This study presents a comprehensive numerical simulation to assess the fire behaviour of a novel composite slab and a new proposal for a simplified method. Three insulation techniques are investigated: a steel shield for the thinner part, a steel shield with the cavity filled with mineral wool, and a mineral wool plate applied from below. The simplified method is proposed to evaluate the fire resistance using new empirical coefficients, recalibrated within the framework of the prEN 1994-1-2 to allow for precise temperature predictions in steel components under standard fire. The numerical model, validated against experimental results, shows that the steel shield insulation extends the time to reach critical temperatures by approximately 25%. In contrast, mineral wool insulation proved to be substantially more effective by reducing temperatures in the UPPER 2 region by up to 89% compared to uninsulated slabs, after 60 min of fire exposure. This significant temperature reduction increases the load-bearing capacity during 60 min of fire exposure by 29%, also resulting in a potential reduction of approximately 22% in carbon emissions. The findings underscore and highlight the potential of these insulation systems to enhance the overall safety and resilience of composite slabs under fire, offering valuable insights for structural fire design.

Keywords: composite slabs; steel decking; fire resistance; fire insulation; finite element modelling; simplified method

Academic Editors: Haifeng Zhao, Konstantinos Tserpes, Salim Belouettar and Marcin Kamiński

Received: 29 July 2025
Revised: 3 September 2025
Accepted: 6 September 2025
Published: 12 September 2025

Citation: Ribeiro, O.G.N.; Piloto, P.A.G.; Gidrão, G.d.M.S. Insulation Strategies to Enhance Fire Resistance in Composite Slabs with Reduced Carbon Emissions. *J. Compos. Sci.* **2025**, *9*, 497. https://doi.org/10.3390/jcs9090497

1. Introduction

Composite slabs with steel decks are highly efficient and lightweight structural solutions compared to conventional reinforced concrete slabs. Given these advantages, this composite slab model has become widely adopted in building projects involving steel structures and high-rise buildings [1]. The composite slab consists of a thin cold-rolled steel deck, typically with thicknesses ranging from 0.6 to 1.2 mm, over which concrete is poured [2]. The concrete is usually reinforced with a light anti-crack mesh and may also include reinforcement bars, typically positioned within the ribs.

The presence of an unprotected steel deck in composite slabs represents a significant disadvantage in terms of fire resistance. When directly exposed to fire, the steel deck's

structural stability can be compromised due to the temperature-induced reduction in strength and stiffness [3]. This issue arises because the steel components are primarily responsible for the load-bearing capacity of the composite slabs, which are crucial for maintaining the structural element stability during a fire. Additionally, these slabs play a vital role in preventing fire from spreading to other compartments within the building.

Fires pose a critical global threat, with over 300,000 annual fatalities attributed to fire-induced burns, predominantly in low- and middle-income countries (LMICs) [4]. Residential fires account for 80% of fire-related deaths in the United States, occurring every 85 s [5,6], while 78% of unintentional fire fatalities in London arise from residential incidents [7]. Human behaviour, particularly unsafe practices, is a primary causative factor [8], exacerbated by evacuation challenges in densely populated residential complexes [6,9]. Fire protection plays a crucial role in building safety, aiming to reduce the likelihood of death, injury, property loss, and environmental damage caused by unwanted fires [10]. Protecting the building's structure and contents is equally vital to prevent the spread of fire and structural collapse, ensuring the structure withstands long enough to evacuate occupants safely [11]. Jiang et al. [12] mentioned that the fire resistance classification of structural elements is typically determined through fire tests, where the element is exposed to a standard fire curve for a specified duration, usually following the fire standard ISO 834 [13]. The fire resistance of an element, measured by its load-bearing capacity (R), insulation (I), and integrity (E), is determined by exposing it to a standard furnace temperature–time curve.

Beyond fire safety, one of the most critical factors is the advancement of low-carbon building practices, as conventional construction releases substantial quantities of carbon into the atmosphere. The construction industry accounts for 40% of global energy consumption and 36% of carbon emissions [14]. Among the industrial sectors, construction is the largest carbon emitter due to the energy-intensive nature of its materials [15]. The production of building materials generates the most carbon emissions (64.5%) over a building's lifecycle. Specifically, the production and use of steel and concrete are the primary contributors to emissions associated with this sector. Notably, steel's recyclability is superior to that of concrete, and the quantity of steel used is significantly lower than that of concrete. Consequently, concrete is the most significant contributor to carbon emissions over a building's lifecycle. To mitigate the carbon footprint of construction, replacing concrete with low-energy materials is imperative.

Recent research highlights the complexities in analysing structural fires in composite slabs. The cooling phase can generate connection failures in frames, and slabs can anticipate collapses [16–18]. Failures in beam–column joints can trigger slab disintegration and fire propagation between floors [19,20], requiring advanced predictive models. Marcílio et al. [1] also noticed that failure may occur during the cooling phase and explored the extension of the simplified EN 1994-1-2 model to natural fire scenarios. However, a broader database is needed, including additional fire curves, different steel slab profiles, mechanical simulations, and experimental tests, to evaluate failure modes [1]. These studies demonstrated how delicate the structures of composite slabs are under fire.

To extend the load-bearing capacity time (R), Fourie (2020) [21] proposed a novel type of insulation for composite slabs with steel decking. The insulation consists of a steel plate, referred to as a steel shield, attached to both ends of the lower regions of the rib, creating an area shielded from direct exposure to fire, as illustrated in Figure 1.

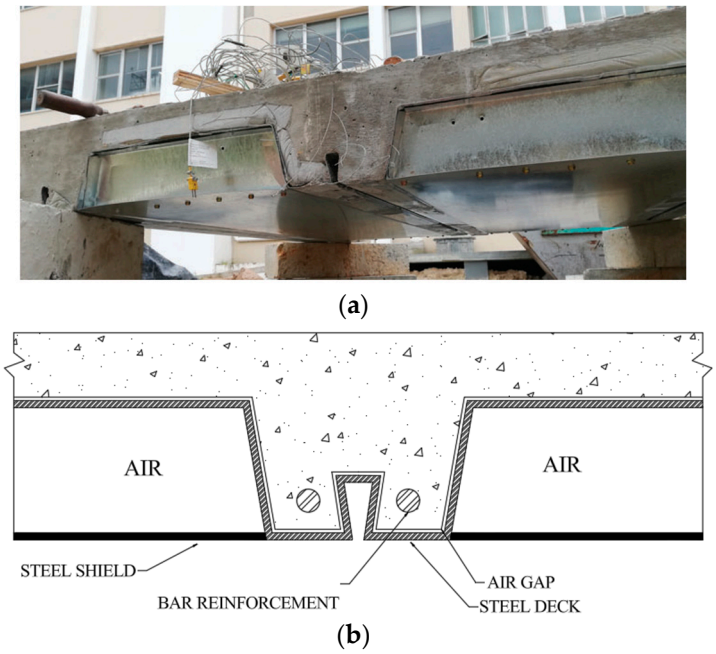

Figure 1. Composite slab model presented by Fourie [21]. (**a**) Slab before test 2. (**b**) Schematic representation of the slab proposed by Fourie.

To analyse the thermal behaviour of this new composite slab, Fourie (2020) [21] conducted two experimental tests, where the difference between the tests lies in the presence of the steel shield. Thermocouples were placed on the lower, web, upper, and rebar, with a fire duration of 90 min for test 1 and 80 min for test 2. The results indicate that including steel shields reduces the unexposed surface average temperature by 16% to 41% [21]. This reduction contributes to a 19.35% decrease in concrete usage [21] and a fire resistance increase of 20 min in the insulation criteria.

Based on the studies conducted by Fourie [21], numerical simulations are presented using the ANSYS software (2024 R2) to demonstrate the load-bearing capacity increase provided by active steel shield insulation. In addition to the steel shield, numerical simulations are conducted using mineral wool, allowing a comparison of temperature and mechanical resistance between steel decks insulated with steel shield, mineral wool, and without insulation. The numerical validation and verification were carried out using the experimental and numerical results, respectively, obtained by Fourie [21]. Mineral wool insulation products are widely used in industrial applications due to their excellent thermal and acoustic insulation properties, non-combustibility, cost-effectiveness, and ease of installation [22]. Its favourable performance per unit volume further supports the selection of this insulation type for various engineering applications.

According to Piloto et al. [23], to improve the accuracy of the numerical model used to simulate the debonding effect of the steel deck from the concrete during a fire, an insulating layer (air gap) with a constant thickness should be introduced between the concrete and the steel deck in the numerical models. In the numerical models presented in this study, an air gap of 0.5 mm is assumed to simulate the debonding effects, aiming to provide a more accurate scenario [1].

This new proposed model is not yet included in the next generation of prEN1994-1-2 [24]. There is a lack of design methods for this new steel deck (bottom re-entrant stiffener in the rib) and a lack of design methods when using insulation materials. The present investigation aims to develop a simplified method that ensures new empirical coefficients, "b_i" for approximating the average temperature in the steel deck components, and new empirical coefficients, "c_i" for approximating the average temperatures in the

rebars. According to Marcílio et al. [1], the equations proposed by EN 1994-1-2 can be used to obtain the average temperatures in steel components as long as the "b_i" and "c_i" coefficients are appropriately calibrated. Moreover, Jiang et al. [25] emphasise that the simplified formulations proposed by EN1994-1-2 [24] overestimate fire resistance and that the moisture content significantly affects the temperature distribution in composite slabs. This study further examines how the integration of insulation systems can enhance carbon emission reduction in the construction of new buildings.

Thus, this paper presents, as its primary innovation, the development and calibration of new empirical coefficients ("a", "b", and "c") for the simplified method of prEN 1994-1-2, specifically adapted for composite slabs with steel decking using thermal insulation systems. These coefficients, calibrated through finite element analysis and validated by experimental results, enable a more accurate prediction of steel component temperatures and load-bearing capacity under standard fire conditions, addressing a regulatory gap for composite steel decks with special rib profiles and insulation materials. Furthermore, an integrated methodology is proposed that correlates the enhancement in fire resistance with the potential for reducing carbon emissions, offering not only a robust tool for fire safety design but also a contribution to sustainability within composite construction.

2. Numerical Model

This research study is based on the Finite Element Method (FEM) using ANSYS software [26], conducted in four solution steps. The first step involves the development of a validated numerical model using the experimental tests conducted by Fourie [21] and the experimental tests developed by CSTB [27], thereby ensuring the accuracy of the numerical model. The second step involves performing an insulation fire analysis in accordance with prEN1994-1-2 [24], measuring the maximum and average temperatures of the unexposed zones, and determining the fire resistance time, following the ISO 834 standard fire curve [13]. The third step consists of a parametric study, running 21 simulations, including 3 types of slabs and 4 types of insulation, to define the optimal values of "b_i" and "c_i", as per prEN1994-1-2 [24], used to determine the temperature in the structural component zones of the composite slabs. The final step involves conducting a simplified load-bearing analysis following the guidelines of prEN1994-1-2 [24], comparing the load-bearing capacity enhancement provided by each type of insulation.

2.1. Geometry and Thermally Affected Regions of the Composite Slab

Figure 2a presents the geometry and temperature-affected regions of the composite steel and concrete slab produced by Voidcon, used by Claasen et al. [28]. This study presents a transient and non-linear thermal analysis of three fire protection types of these composite slabs (steel shield, steel shield with mineral wool above and steel shield with mineral wool plates below).

The composite slab insulation, protected by a steel shield, creates an air cavity in the UPPER 2 and WEB 2 regions, preventing these areas from being directly exposed to fire [21]. The second insulation was also assumed to be made using mineral wool in the cavity region formed by the steel shield. The third proposed insulation involves the addition of a mineral wool board beneath the steel plate, as illustrated in Figure 2b. Within the resulting cavity, radiation and convection phenomena will occur, with the insulation thickness (hi) being adjustable. For the parametric study, hi values of 5, 10, 20, and 30 mm were employed.

In the present geometry, as shown in Figure 2a, there are two distinct regions: a general trapezoidal region (T), composed of the lower region, WEB 2, and UPPER 2, and a re-entrant region (R), formed by WEB 1 and UPPER 1. Each region has unique dimensions, which are critical for calculating the average temperature within its respective elements

using the simplified method [24]. This approach relies on accurately determining the view factors, as they directly influence the temperature field.

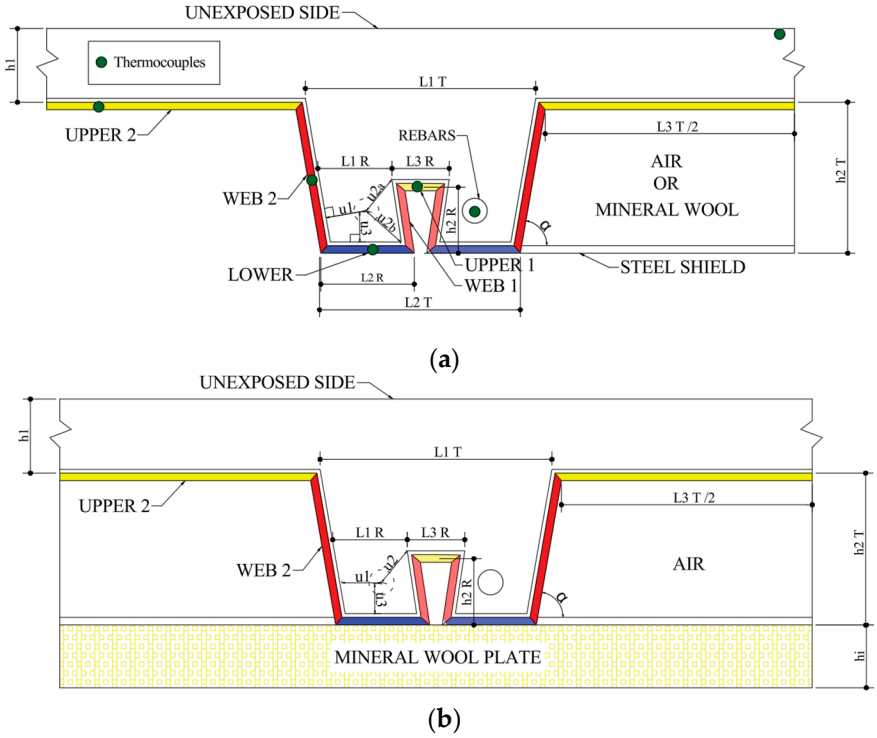

Figure 2. (**a**) Dimensions and zones of the Voidcon slab. (**b**) Dimensions of the Voidcon slab with mineral wool insulation plate. Adapted from [21].

Table 1 presents three different types of Voidcon steel decks and the geometry used for this investigation. The concrete cover has been considered constant and equal to 65 mm.

Table 1. Dimensions of the slab produced by Voidcon.

	VP 50	**VP115**	**VP 200**
L1 R (mm)	30	50	85
L2 R (mm)	55	75	110
L3 R (mm)	25	25	25
L1 T (mm)	165	200	300
L2 T (mm)	115	150	230
L3 T (mm)	250	400	460
h1 (mm)	65	65	65
h2 T (mm)	50	115	200
h2 R (mm)	50	50	50
u1 (mm)	24	37	47
u2 (mm)	32	32	47
u3 (mm)	25	25	25
α (°)	63.40	77.73	80.07

To calculate the temperature effect in each region, 10 points were collected, and the arithmetic average temperature was determined.

The temperature field is determined by solving the heat conservation equation inside the solid parts (see Equation (1)) through the discretisation of the domain using a finite element mesh as illustrated in Figure 3. The material properties are temperature-dependent, and the solution method is incremental and iterative, using a time increment of 60 s, reducible to 1 s if required. The convergence criterion was based on heat flow, with a tolerance of 10^{-3} and a minimum reference value of 10^{-6} W.

$$\rho(T)C_p(T)\frac{\partial T}{\partial t} = \nabla\cdot(\lambda(T)\nabla T) \quad (1)$$

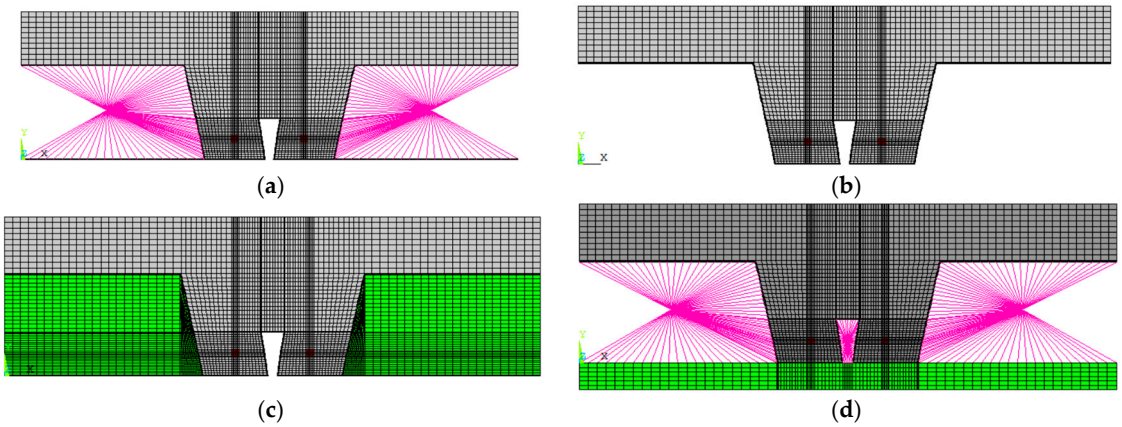

Figure 3. Mesh size for VP 115. (**a**) Composite slab with steel shield insulation. (**b**) Composite slab without insulation. (**c**) Composite slab with mineral wool and steel shield insulation. (**d**) Composite slab with mineral wool plate and steel shield insulation.

T represents the temperature of each material [K], $\rho(T)$ is the specific mass [kg/m^3], $C_p(T)$ is the specific heat [J/kgK], λ (T) is the thermal conductivity [W/mK], t is the time [s], and ∇ is the gradient in 2D space. Equation (1) is based on the heat flow balance for the infinitesimal material volume in each spatial direction.

The boundary conditions are defined in the exposed and unexposed sides of the composite slabs, using Equation (2). The exposed surface is submitted to radiation and convection, while convection is assumed in the unexposed surface with an appropriate convection coefficient to consider the radiation effect. The cavity region is also submitted to convection and radiation, using Equation (2) again, but using average convection coefficients between the exposed and unexposed surfaces. The average view factor ∅ was determined for each region. The emissivity of the material exposed to radiation ε_m depends on the surface material and the emissivity of the flames ε_f equals 1. The Stefan–Boltzmann coefficient is σ. The bulk temperature is defined by T_∞.

$$-(\lambda(T)\nabla T)\cdot\vec{n}. = \alpha_c(T_\infty - T) + \varnothing\varepsilon_m\varepsilon_f\,\sigma\left(T_\infty^4 - T^4\right) \quad (2)$$

A two-dimensional model is presented, assuming no temperature variation through the span of the composite slab and neglecting the temperature effect near the supports. The temperature field is determined by the weighted residual method, using Galerkin approximation, ending in the solution of a set of algebraic equations. Based on previous 3D, thermal, and mechanical simulations developed by the authors, the 2D finite element analysis is justified by the slab's uniform cross-section, which minimises longitudinal heat flow, concentrating it in the 2D analysis of the cross-section.

2.2. Two-Dimensional Finite Element Mesh

This study used the PLANE55 [26,29] finite element for two-dimensional conduction thermal analysis to evaluate heat conduction in planar regions (cross-section of the composite slab). This finite element has four nodes, one degree of freedom (temperature) per node, and assumes linear interpolating functions and a full Gauss (2 × 2) integration method. The element supports both transient and steady-state analyses, including convection and radiation effects.

The finite element LINK31 [26,29] models heat exchange by radiation between surfaces. This two-node finite element incorporates parameters such as radiation area, geometric view form factor, and emissivity, applying the Stefan–Boltzmann Law to calculate radiation heat flow between two nodes. The non-linearity is solved iteratively using the Newton–Raphson method, with emissivity defined as either constant or temperature-dependent. This element has no interpolating function or numerical integration, and uses a direct formula to determine the heat flow [W] by radiation; see Equation (3).

$$q\,[W] = \sigma \times \varepsilon_R \times \varnothing \times A \times \left(T_i^4 - T_j^4\right) \tag{3}$$

The resultant emissivity is defined by $\varepsilon_R = \varepsilon_f.\varepsilon_m$. The area of influence used for each finite element depends on the position of the nodes and should be previously defined [26].

The finite element LINK34 [26,29] simulates uniaxial thermal convection between nodes, featuring a non-linear film coefficient depending on temperature or time. The convective heat transfer rate is determined based on the film coefficient, convection area, and possible empirical coefficients (not used here). This element also has no interpolating function or numerical integration, and uses a direct formula to determine the heat flow by convection; see Equation (4). This equation depends on the convection coefficient used in the cavity region (average value) and on the area of influence defined between the two nodes. This formula is also prepared to use an empirical coefficient E, herein assumed as 1.

$$q\,[W] = \alpha_c \times A \times E \times \left(T_i - T_j\right) \tag{4}$$

Figure 3 presents the finite element mesh adopted for the VP50, VP115, and VP200 configurations, highlighting three fire scenarios. Figure 3a presents a composite slab with steel shield insulation, where LINK31 and LINK34 elements are employed to simulate the heat transfer within the air cavity. Figure 3b presents a composite slab without insulation. Figure 3c presents a composite slab with mineral wool and steel shield insulation, both discretised using PLANE55 elements. Figure 3d presents a composite slab with a mineral wool plate and steel shield insulation, both discretised using PLANE55 elements and LINK31 and LINK34 elements, which are employed to simulate the heat transfer within the air cavity. The mesh distribution and density are optimised to capture the critical temperature gradients in each configuration accurately. The thinner regions are modelled with a minimum of three finite elements, regarding the linear interpolating functions used in PLANE55.

The air gap modelling is produced using thermal conduction using a planar region in ANSYS with PLANE55 to simulate the debonding effect between concrete and steel. The selection of a constant debonding thickness of 0.5 mm follows sensitivity analyses conducted by Balsa et al. [30], which determined this value to provide an optimal balance between model accuracy and computational efficiency for simulating debonding separation behaviour under fire conditions.

2.3. Boundary Conditions

Heat flux by convection and radiation is applied as a primary thermal boundary condition in accordance with EN1991-1-2 [31]. The convection coefficient of 25 W/m^2K is assigned to the fire-exposed side, and 9 W/m^2K to the unexposed side, accounting for radiative effects. The flame emissivity factor of 1.0 is applied with a Stefan–Boltzmann constant of 5.67×10^{-8} W/m^2K^4, consistent with previous studies [32–34]. The core temperature on the exposed side was defined using the ISO834 standard fire time–temperature curve, while the non-exposed side was assumed to maintain a constant temperature of

20 °C. Figure 4 illustrates the details of the thermal boundary conditions applied to the steel deck with the steel shield insulation model.

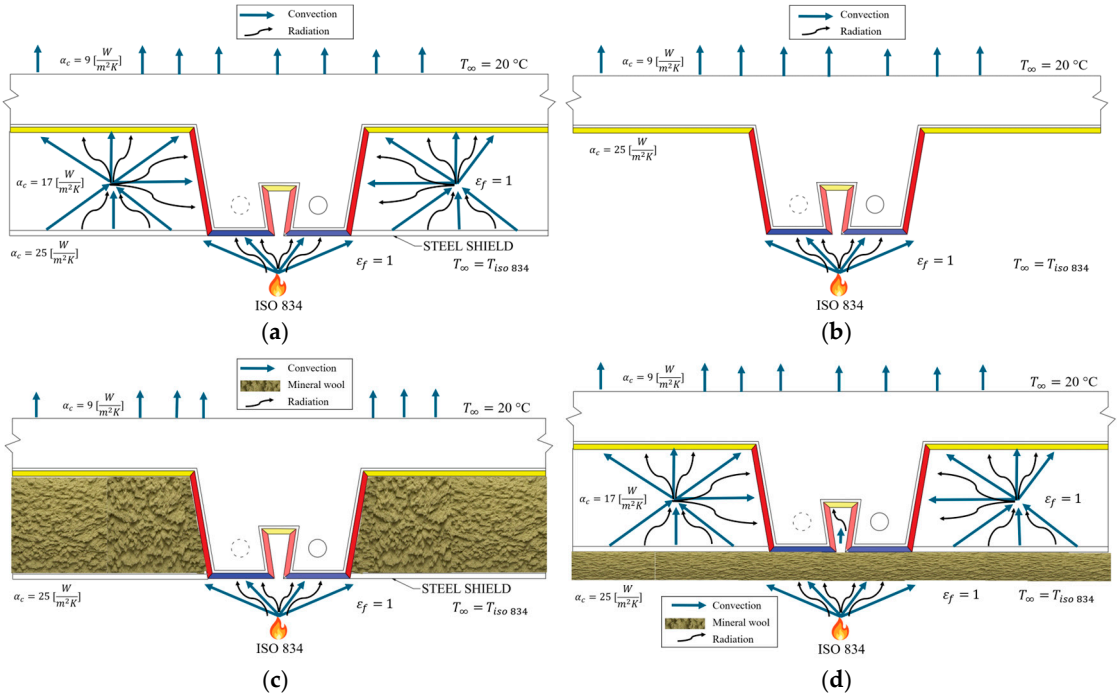

Figure 4. Thermal boundary conditions. (**a**) Slab with steel plate insulation. (**b**) Slab without insulation. (**c**) Slab with mineral wool insulation. (**d**) Slab with mineral wool plate [13].

The methodological approach adopted in this investigation maintains the bulk temperature on the unexposed side at 20 °C. According to previous experimental temperature measurements [32], this value increases with time, but keeps the temperature very low. Moreover, this assumption provides conservative fire resistance results.

The thermal analysis is conducted as a transient non-linear analysis, configured with full option settings.

3. Simplified Calculation Method

The simplified calculation method used for the (R) criterion presented by prEN1994-1-2 [24] can be applied to simply supported composite slabs when exposed to standard fire ISO-834 [13]. To determine the bending moment capacity of the composite slab (sagging moment), this standard requires the temperature for each component of the steel section (top flange, web, and bottom flange) to be calculated for each required fire rating, according to Equation (5). For the reinforcement components, the temperature θ_s is determined using Equation (6). The temperatures θ_a and θ_s are given in °C. Other required parameters are defined by Equation (7) to Equation (8).

The insulation's fire resistance is determined by Equation (9), and also depends on a series of geometric parameters. The parameter $\varnothing$ is dimensionless and represents the view factor of the steel section component, as given by Equations (10) and (11). The length L_3 is the distance within the ribs and u_3 represents the distance from the centre of the reinforcement to the bottom flange in mm, as shown in Figure 2.

$$\theta_a = b_0 + b_1\frac{1}{L_3} + b_2\frac{A}{L_r} + b_3\varnothing + b_4\varnothing^2 \tag{5}$$

$$\theta_s = c_0 + c_1\frac{u_3}{h_2} + c_2 z + c_3\frac{A}{L_r} + c_4\alpha + c_5\frac{1}{L_3} \tag{6}$$

The z factor represents the position of the reinforcement relative to the slab rib using u_{2a}, as shown in Figure 2 and used in Equation (7), given in $mm^{-0.5}$. α represents the angle between the web component of the steel formwork and the horizontal direction in degrees (°), as shown in Figure 2. The ratio A/L_r is the rib geometry factor and represents the relationship between the concrete volume and the area exposed per metre of length of the steel formwork rib, given in mm, and its calculation is performed using Equation (8).

$$\frac{1}{z} = \frac{1}{\sqrt{\frac{1}{u_1}}} + \frac{1}{\sqrt{\frac{1}{u_2}}} + \frac{1}{\sqrt{\frac{1}{u_3}}} \tag{7}$$

$$\frac{A}{L_r} = \frac{h_2\left(\frac{L_1+L_2}{2}\right)}{L_2 + 2\sqrt{h_2^2 + \left(\frac{L_1-L_2}{2}\right)^2}} \tag{8}$$

The coefficients "a_i", "b_i", and "c_i" represent the empirical coefficients used by prEN1994-1-2 [24], which depend on the type of concrete (NWC or LWC) and on the standard fire rating. Equations (5) and (6) allow for estimating the average temperatures that affect the strength reduction coefficients in all steel deck components and rebars, consequently enabling an accurate estimation of the load-bearing capacity criteria after a specific time (fire rating). The load-bearing capacity criteria (R) will be based on the reduction coefficients applied to the yield strength of each component.

To determine the insulation fire resistance (I) time in minutes, Equation (9) is used, which employs the empirical coefficients "a_i" generally used by prEN1994-1-2 [24].

$$t_i = a_0 + a_1 h_1 + a_2 \varnothing_{UPPER\ 2} + a_3 \frac{A}{L_r} + a_4 \frac{1}{L_3} + a_5 \frac{A}{L_r}\frac{1}{L_3} \tag{9}$$

The view factor ($\varnothing$) quantifies the radiation received by an exposed surface. In numerical simulations, specific considerations must be considered and used. For instance, the lower flange is assumed to have a view factor of $\varnothing_{LOWER} = 1$ because it is oriented parallel to and directly exposed to the fire. In contrast, the other components, which are not directly exposed, require their average view factors to be calculated using Equations (10) and (11). This calculation is based on the Hottel crossed-strings method [35]. Table 2 represents the view factor for the thermal zones of all the slabs to be used in the numerical model, corresponding to the respective regions.

$$\varnothing_{UPPER} = \frac{\left(\sqrt{h_2^2 + \left(L_3 + \frac{L_1-L_2}{2}\right)^2} - \sqrt{h_2^2 + \left(\frac{L_1-L_2}{2}\right)^2}\right)}{L_3} \tag{10}$$

$$\varnothing_{WEB} = \frac{\left(\sqrt{h_2^2 + \left(\frac{L_1-L_2}{2}\right)^2} + (L_3 + L_1 - L_2) - \sqrt{h_2^2 + \left(L_3 + \frac{L_1-L_2}{2}\right)^2}\right)}{2\sqrt{h_2^2 + \left(\frac{L_1-L_2}{2}\right)^2}} \tag{11}$$

Table 2. View factors used for the composite slabs produced by Voidcon® [36].

	VP 50	**VP115**	**VP 200**
$\varnothing_{LOWER}$	1	1	1
$\varnothing_{WEB\ 2}$	0.697	0.480	0.480
$\varnothing_{UPPER\ 2}$	0.930	0.780	0.712

Table 2. *Cont.*

	VP 50	VP115	VP 200
$\varnothing_{WEB\ 1}$	0.058	0.058	0.058
$\varnothing_{UPPER\ 1}$	0.064	0.064	0.064

4. Materials

The thermal conductivity and specific heat from the steel parts are depicted in Figure 5a, and defined according to the standard FprEN1993-1-2 [37]. Additionally, the emissivity of the steel was obtained from Table 3, using the values for the hot-dip-galvanised deck, which is different from carbon steel. For the density of both the steel deck and rebars, a value of 7850 kg/m^3 is assumed at room temperature and remains constant at elevated temperatures. The steel grade used for the steel deck is ISQ 23 Grade 275 galvanised steel, with presents a characteristic strength of 230 MPa; the reinforcement bar steel has a characteristic strength of 450 MPa. The rebars used for all the slabs have a diameter of 10 mm. The thermal conductivity and specific heat of normal-weight concrete are depicted in Figure 5b, and defined according to the standard prEN1994-1-2 [24]. The density of the concrete starts at a temperature of 20 °C with a value of 2300 kg/m^3 and decreases to 2024 kg/m^3 when reaching a temperature of 1200 °C. The thermal properties of air are also non-linear, as depicted in Figure 5c, as derived from data presented by Çengel [35]. Based on prEN 1995-1-2 [38], the thermal properties of mineral wool manufactured by Rocterm® [39], PN 70, with a density of 70 kg/m^3, presents the thermal properties depicted in Figure 5d.

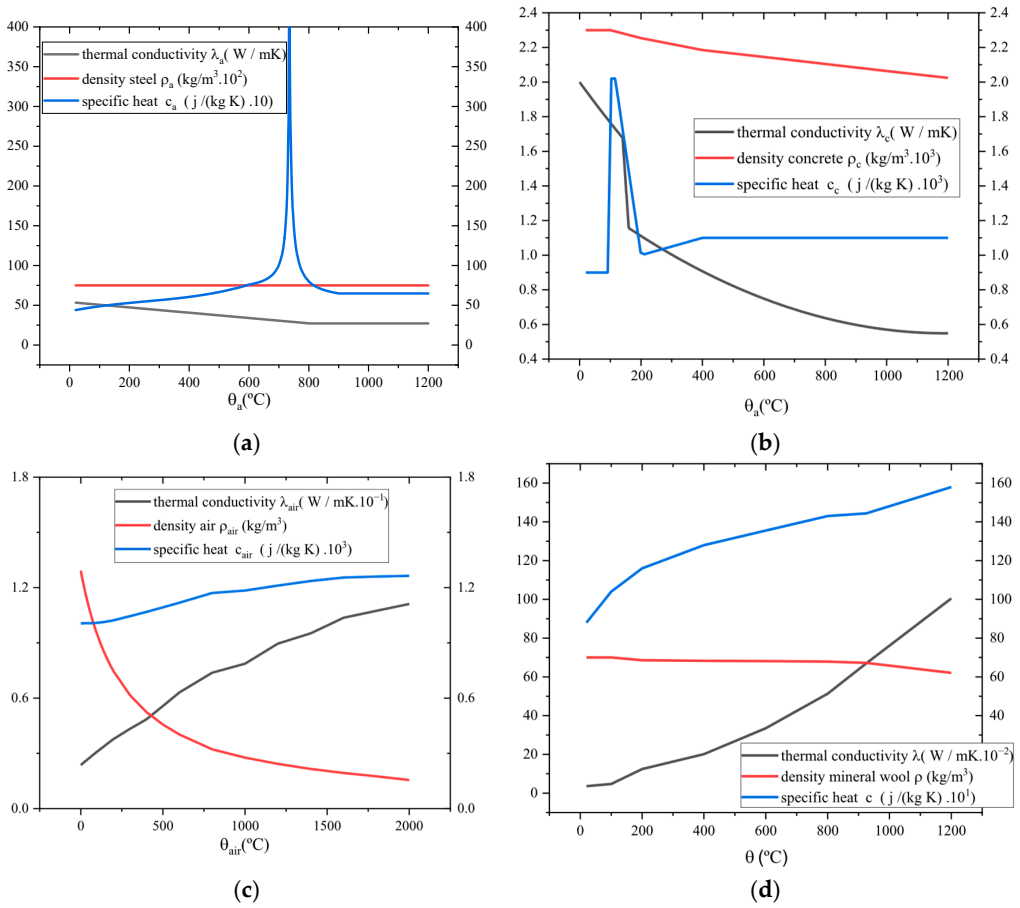

Figure 5. Variation in thermal material properties at elevated temperatures: (**a**) steel for steel deck and rebars; (**b**) normal-weight concrete; (**c**) air; (**d**) mineral wool.

Table 3. The emissivity of steel.

Type of Steel	ε_m ($\leq$500 °C)	ε_m (>500 °C)
Carbon steel	0.7	0.7
HDG steel [a]	0.35	0.7

[a] Steel that has been hot-dip-galvanised according to EN ISO 1461(2022) [40] and with steel composition according to Category A or B of ISO 14713-2 (2019) [41].

5. Results

The results of the advanced thermal and simplified structural analyses encompass the behaviour of composite slabs under fire conditions, the performance of the proposed insulation systems, and the load-bearing capacity of the structures over time. The comparison between experimental results, Figure 6, and numerical simulations demonstrates the validation of the models and the calibration of the empirical coefficients "a_i", "b_i", and "c_i", detailing the validation of the numerical model, the analysis of insulation criteria, and the parametric study of mechanical performance during fire exposure.

Figure 6. Specimen 2, obtained from Fourie [21], after the test was completed.

5.1. Numerical Validation

Figure 7a compares the temperatures recorded in the unexposed region of the VP115 composite slab with the steel shield, considering the experimental test results obtained both by Fourie [21] and by this investigation using ANSYS. Additionally, Figure 7b compares Fourie's experimental results with the numerical results from this investigation for the UPPER 2 and WEB 2 zones. It can be noted that, for these regions, the numerical results show good agreement with the experimental results, as illustrated in Figure 7. The results are presented in Figure 7, which displays Fourie's experimental temperature measurements alongside the numerical prediction. According to Fourie [21], the difference between numerical and experimental results is due to the formation of an air gap during the initial periods of the experiment, a phenomenon also noted by Piloto et al. (2020) [23]. Figure 7c presents the temperature field of the validation test at 60 min for VP 115 with a steel shield.

The air gap size is assumed to be a constant average value, valid throughout the entire interface between steel and concrete. The debonding effect results from the difference in thermal expansion between these two materials. The actual air gap size in the experiments is expected to increase depending on the fire event. The numerical results slightly underestimate the temperature of the unexposed concrete region and overestimate the steel temperature in the UPPER 2 region.

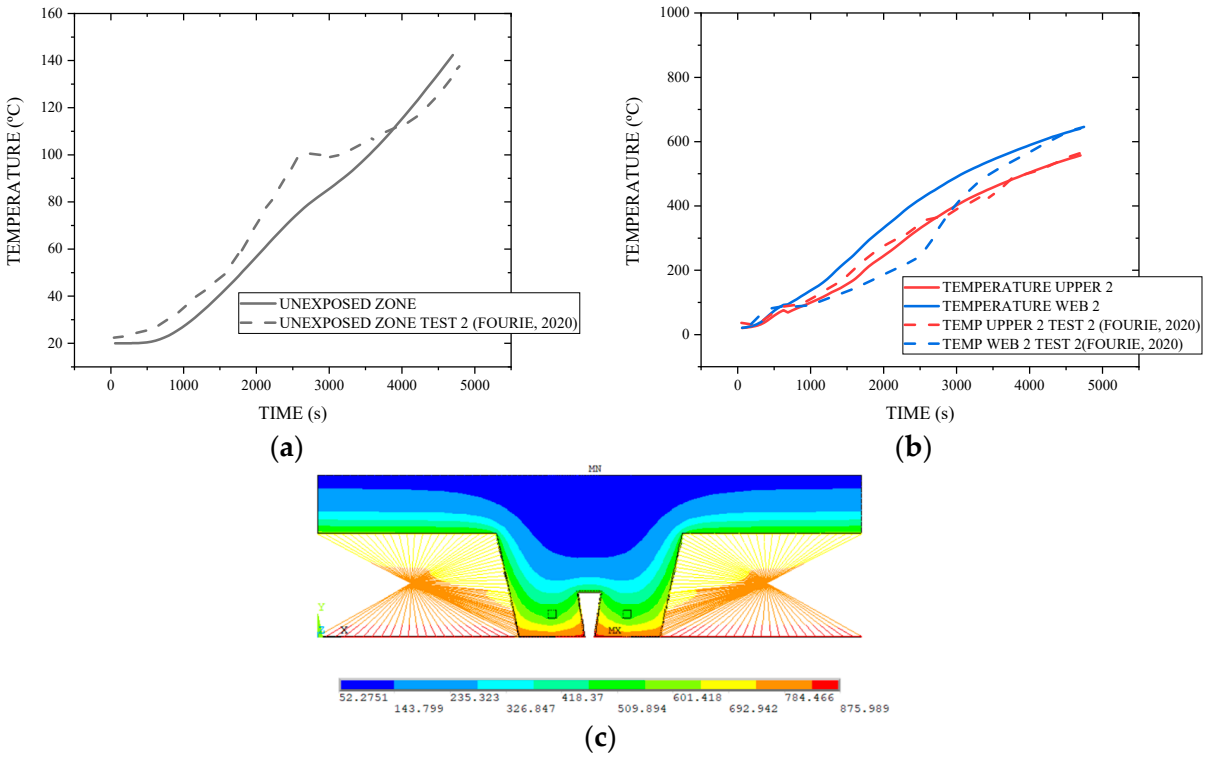

Figure 7. Comparison of the experimental results obtained by Fourie [21] with those obtained using the ANSYS model in this study. (**a**) Unexposed zone; (**b**) steel sheet trapezoidal zones; (**c**) temperature field after 60 min.

The root mean square errors (RMS) are presented in Table 4 for the absolute and relative difference. These values were determined between the numerical model and the experimental results throughout the simulation for the WEB 2, UPPER 2, and unexposed zones. This value reflects the accuracy of the computation model, considering that at any time after the first 10 min of any standard fire test, the temperature recorded by any thermocouple in the furnace should not differ from the corresponding temperature of the standard temperature–time curve by more than 100 °C [42].

Table 4. Root mean square error (°C) between experimental and numerical results of VP 115 with steel shield.

REGION ZONE	RMS (°C)	RMS (%)
WEB 2	82.1	18
UPPER 2	18.1	6
UNEXPOSED	10.4	15

An experimental test report from the structures, safety and fire department at CSTB [27] was used to validate models utilising mineral wool. This report used the COFRADAL 200 steel deck, as shown in Figure 8a. The analysis was conducted using the ANSYS software, with the finite element PLANE55 [26], illustrated in Figure 8b. The boundary conditions applied were identical to those used for the first validation (composite slab VP 115), with convection coefficients of 25 W/m^{2}K for the exposed face and 9 W/m^{2}K for the unexposed face, in accordance with EN 1991-1-2 [31]. A constant view factor of 1 was utilised for radiation, with an emissivity coefficient of 0.7 (assuming carbon steel). The ISO-834 standard fire curve [13] was applied.

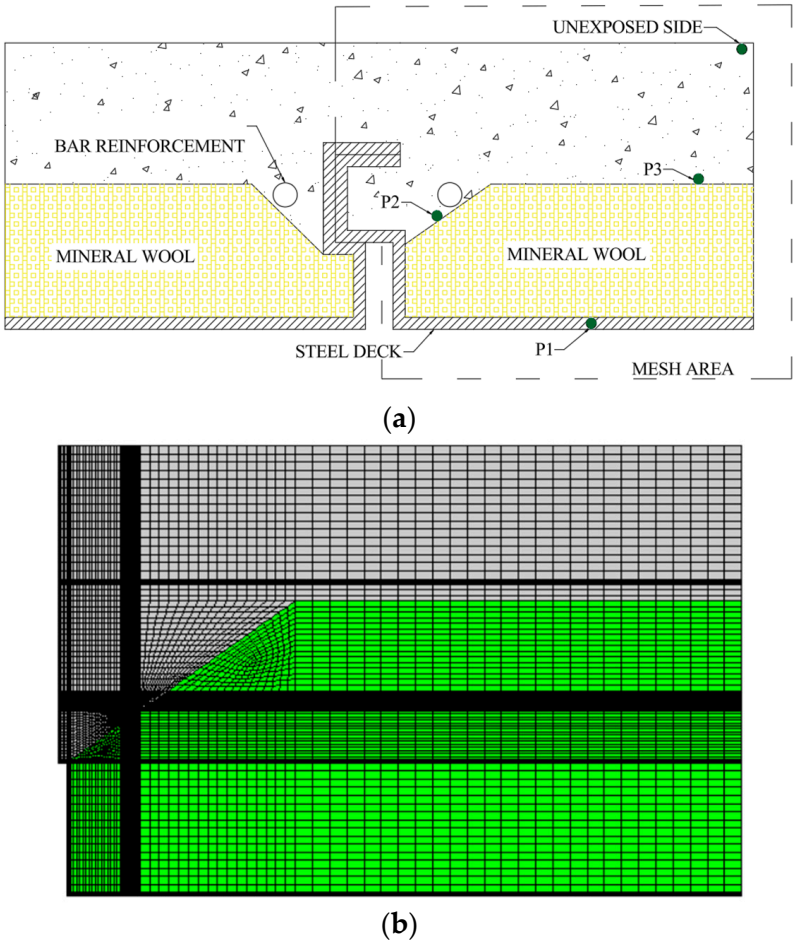

Figure 8. (**a**) Thermocouples used in the COFRADAL 200 experimental test [27]; (**b**) mesh size of COFRADAL 200 in ANSYS.

Figure 9a shows the comparison of the temperature evolution at points P1 and P2 between the experiment conducted by CSTB [27] and the numerical simulations performed using ANSYS software. Figure 9b, meanwhile, presents the comparison of the temperature history at point P3 and on the unexposed face. Table 5 presents the RMSE values. The highest value occurs at P1; however, it remains below the 100 °C threshold limit [42]. The other analysed points exhibit low values, demonstrating the reliability of the numerical model and thus enabling a parametric study. Figure 9c shows the temperature field at 60 min from that validation.

Table 5. Root mean square error (°C) between experimental and numerical results of COFRADAL 200.

REGION ZONE	RMS (°C)	RMS (%)
P1	54.5	7
P2	20.3	8
P3	10.3	12
UNEXPOSED SIDE	1.4	3

The discrepancies observed between the numerical and experimental results, namely the overestimations and underestimations, can be attributed to uncertainties in the precise location of the thermocouples, the use of effective thermal properties rather than measured values incorporating degradation, as well as the effect of material moisture evaporation and migration, which are responsible for the higher or lower temperature plateau.

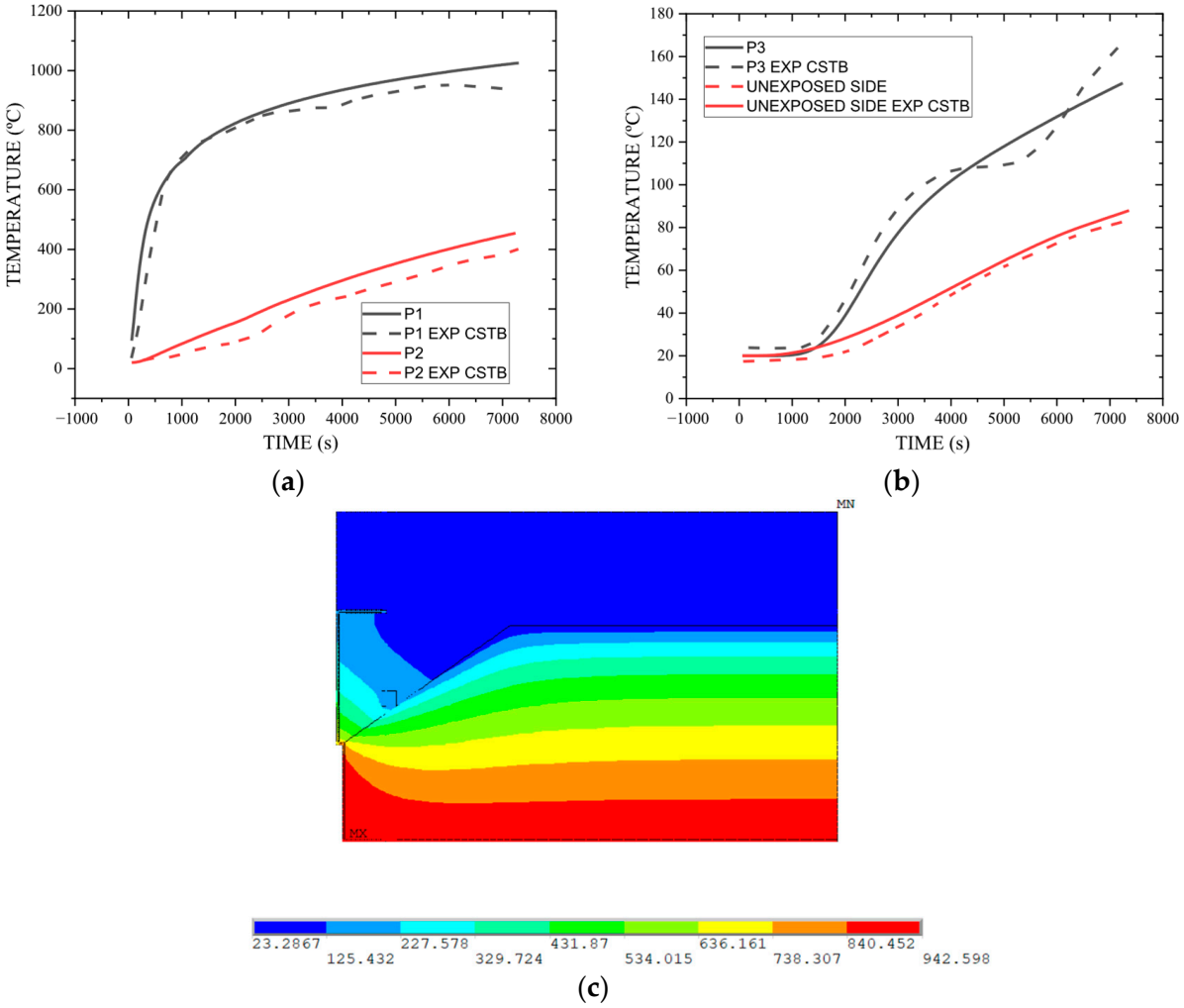

Figure 9. Comparison of the experimental results obtained by CSTB [27] with those obtained using the ANSYS model in this study. (**a**) P1 and P2; (**b**) P3 and UNEXPOSED side; (**c**) temperature field after 60 min.

5.2. Insulation Fire Resistance (I)

Table 6 presents the results for the fire resistance (criterion 'I') for the composite slabs and their insulation types. This fire resistance criterion is determined with respect to the average temperature rise, 140 °C above the initial average temperature (T0), or with respect to the maximum temperature rise, 180 °C above the initial average temperature (T0), on the unexposed surface of the slab. The lowest value between the two limits determines the fire resistance, according to EN1363-1 (2020) [42]. prEN1994-1-2 [24] also defines the minimum effective thickness as a function of standard fire resistance.

After four hours of simulation using the ISO 834 curve [13], the results showed a time gain for the maximum and average temperatures on the unexposed surface compared to the composite slab without insulation. The steel shield insulation is used in three types of composite slabs, resulting in a time gain of approximately 25% for the maximum temperature criterion in all slabs. The use of mineral wool in the cavity region of the composite slab VP50 with h2 = 50 mm shows a total time gain of 43% compared to the composite slab without insulation. The composite slabs VP115 and VP200 with mineral wool, even after four hours, did not reach the temperature limit for the insulation criterion. The composite slab with mineral wool plate insulation showed significantly improved fire resistance (I), increasing proportionally to the insulation thickness (hi). On average, if one

is using hi of 30 mm, the composite slab exhibits a 65% enhancement in fire resistance compared to non-insulated composite slabs.

Table 6. Time limit for the fire resistance (I) criteria.

Type of Slabs	Insulation Type		T_0 + 180 (min)	T_0 + 140 (min)
VP 50	without insulation		61	66
	steel shield		78	77
	mineral wool		109	113
	mineral wool plate	hi = 5 mm	96	99
		hi = 10 mm	114	114
		hi = 20 mm	143	143
		hi = 30 mm	180	169
VP 115	without insulation		61	83
	steel shield		80	97
	mineral wool		333 [a]	276 [a]
	mineral wool plate	hi = 5 mm	100	113
		hi = 10 mm	120	133
		hi = 20 mm	155	171
		hi = 30 mm	191	222
VP 200	without insulation		62	102
	steel shield		81	107
	mineral wool		449 [a]	501 [a]
	mineral wool plate	hi = 5 mm	103	143
		hi = 10 mm	124	157
		hi = 20 mm	163	210
		hi = 30 mm	200	255 [a]

[a] Exceeded the fire rating of 240 min for criterion I according to standard EN 13501-2 [43].

New empirical coefficients "a_i" were determined to calculate the fire resistance insulation time (in minutes) according to the standard prEN1994-1-2 [24]. The simplified method uses Equation (9) to derive these coefficients for insulation fire resistance. The calculation is made using a non-linear evolutionary solver [44], implemented in Excel. Table 7 presents the newly established coefficients "a_i".

Table 7. New coefficients "a_i" proposed to determine the insulation fire resistance in composite steel deck under fire curve ISO 834 for a steel shield and mineral wool insulation.

	a_0 (min)	a_1 (min/mm)	a_2 (min)	a_3 (min/mm)	a_4 (mm min)	a_5 (min)
Steel shield model	−28.79	1.72	−3.21	0	−734.50	7.90
Mineral wool model	−1207.42	19.71	−33.10	5,61	−26,611.50	0.008

The proposed equation to determine the insulation time (t_i) of mineral wool plates retains the fundamental structure of Eurocode 4 Part 1-2 [24], employing a linear combination of geometric and thermal parameters to estimate fire resistance. However, the formulation introduces two critical terms explicitly dependent on the insulation thickness (*hi*), addressing the limitations in the Eurocode methodology for systems incorporating

mineral wool. The general form of the equation aligns with the EN1994-1-2 framework, and is presented in Equation (12).

$$t_i = a_0 + a_1 h_1 + a_2 \varnothing_{UPPER\ 2} + a_3 \frac{A}{L_r} + a_4 \frac{1}{L_3} + a_5 \frac{A}{L_r} \frac{1}{L_3} + a_6 \log\left(\frac{hi}{1}\right) + a_7 * hi^{\frac{1}{h2^2}} \quad (12)$$

The coefficients a_0 to a_5 used in Equation (12) are derived from the steel shield model (Table 6), ensuring continuity between insulation configurations. This methodology ensures that the equation reduces to the steel shield model when the mineral wool insulation thickness hi is zero, maintaining consistency across systems. New coefficients a_6 to a_7 are presented in Table 8, facilitating the calculation of the insulation fire resistance for composite steel decking systems incorporating mineral wool plates.

Table 8. New coefficients "a_i" proposed to determine the time of insulation in steel deck under fire curve ISO 834 for mineral wool plate insulation.

	a_6 (min)	**a_7 (min)**
Mineral wool plate model	112.6	−82.1

5.3. Parametric Study and New Proposal

Figure 10 illustrates the temperature field for the composite slab VP115, under standard fire exposure ISO 834 [13], when using three different insulation types. These results correspond to a fire duration of two hours (7200 s), with the analysis conducted for a concrete thickness of h1 = 65 mm.

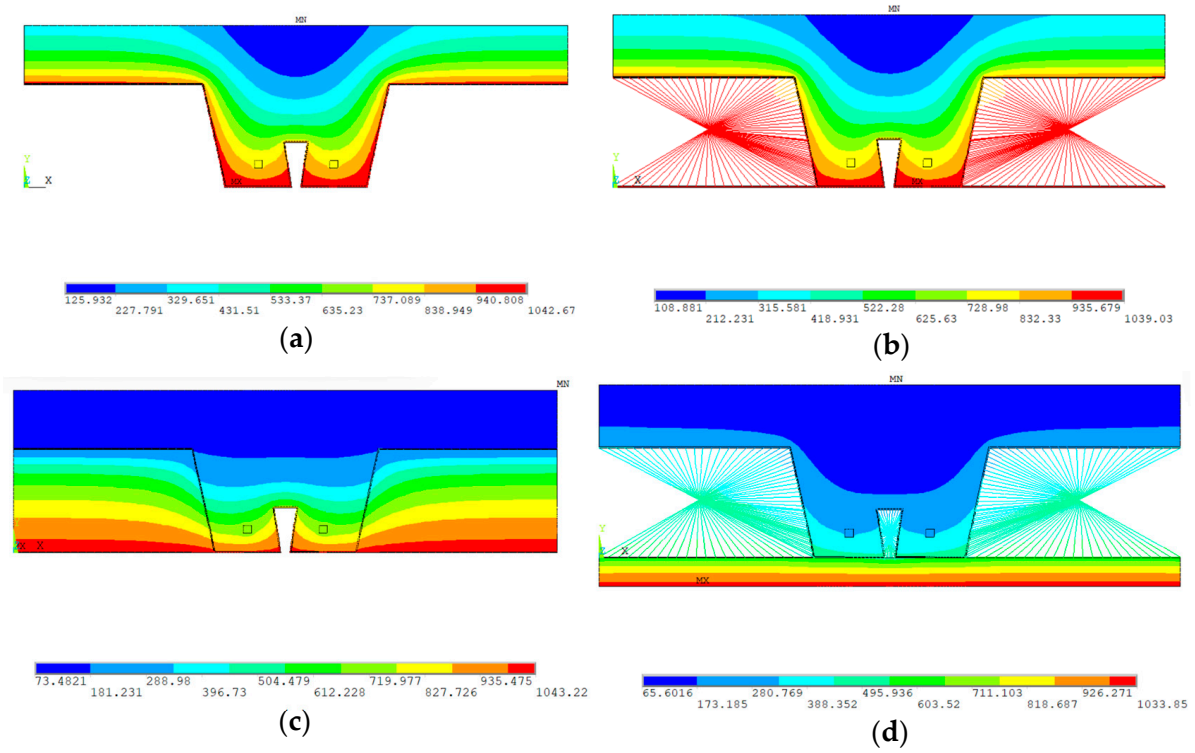

Figure 10. Temperature field over the composite slabs under ISO 834 curves for the same h_1 = 65 mm for a time equal to 7200 s: (**a**) VP115 without insulation; (**b**) VP115 with steel shield; (**c**) VP115 with mineral wool; (**d**) VP115 with mineral wool plate hi = 30 mm.

Furthermore, Figure 11 presents the temperature history, from 0 to 7200 s, at the UPPER 2 region, for three different geometries of composite slabs, each with a distinct insulation system, all considering the same concrete thickness of h1 = 65 mm under the ISO834 standard for fire exposure.

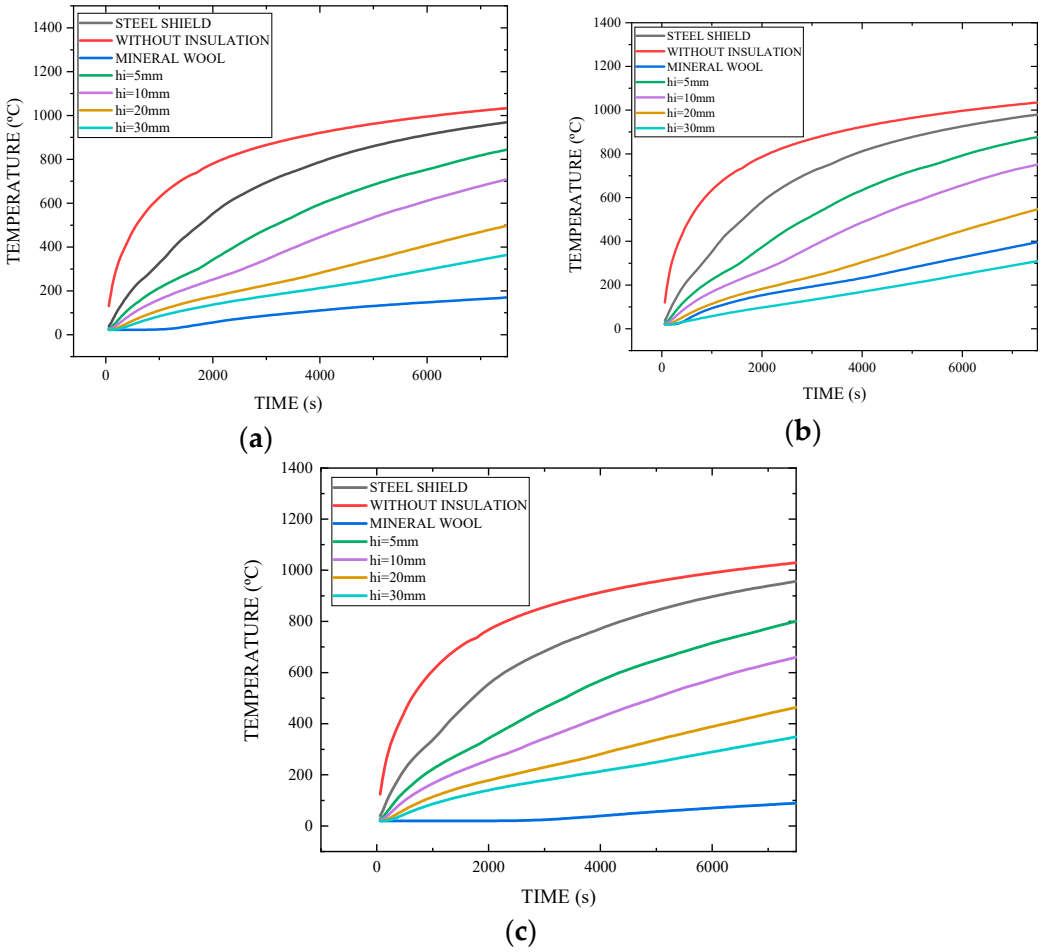

Figure 11. Comparison of temperature history in the UPPER 2 zones for the composite slabs under ISO834 fire standard for the same h1 = 65 mm for a time from 0 to 7200 s: (**a**) VP115; (**b**)VP50; (**c**) VP200.

The numerical results obtained from ANSYS software are averaged for each component of the composite slabs. The average temperatures are determined for the lower flange (LOWER zone), the web (WEB zone), and the upper flange (UPPER zone). Coefficients "b_i" and "c_i" are introduced to determine the average temperatures in the steel deck components insulated with steel shield and mineral wool, as well as in the reinforcing bars, considering the composite slabs under these fire conditions. The proposed coefficients are obtained using Excel, which minimises the sum of the absolute differences between the numerical temperatures (obtained from the steel components in the parametric study) and the temperatures calculated by the model corresponding to Equation (5) or Equation (6). This minimisation is also performed using the non-linear evolutionary solver [44], available in the Excel SOLVER tool. The tool iteratively adjusted the values of "b_i" and "c_i" with the objective of achieving the lowest possible absolute error between the simplified method (with the new coefficients) and the numerical results.

Table 9 compares the effect of the steel shield and mineral wool insulation for the VP115 composite slab. The mineral wool reduces UPPER 2 temperatures from 906.3 °C (without insulation) to 99.3 °C (3600 s), while the steel shield achieves 751.0 °C. Similar

efficiency is observed in WEB 2 (e.g., 888.8 °C vs. 391.3 °C at 3600 s). The lower region shows negligible differences (<1%) between methods. The mineral wool has superior thermal resistance in critical zones, highlighting its suitability for structural fire protection. The VP50 and VP200 composite slab geometries perform similarly to VP115.

Table 9. Comparison in temperature between the model without insulation and the model with a steel shield for VP115.

Time (min)	Region	Without Insulation (°C)	Steel Shield (°C)	Difference % (a)	Mineral Wool (°C)	Difference % (b)
60	LOWER	923.2	920.6	0.27	917.8	0.65
	WEB 2	888.8	778.9	12.36	391.3	44.00
	UPPER 2	906.3	751.0	17.13	99.3	89.07
90	LOWER	994.4	990.6	0.40	987.6	0.70
	WEB 2	966.9	897.5	7.14	491.2	49.14
	UPPER 2	979.3	881.1	10.01	135.9	86.21
120	LOWER	1039.7	1038.1	0.09	1035.1	0.384
	WEB 2	1018.7	969.7	4.81	567.2	44.20
	UPPER 2	1025.9	958.1	6.60	163.2	84.07

(a) Difference between slabs without insulation and with steel shield. (b) Difference between slabs without insulation and with mineral wool.

Table 10 summarises the temperature differentials between the non-insulated configuration and the mineral wool plate-insulated composite slab.

Table 10. Comparison in temperature between the model without insulation and the model insulated with mineral wool plate hi = 30 mm for VP115.

Time (min)	Region	Without Insulation (°C)	Mineral Wool Plate hi = 30 mm (°C)	Difference %
60	LOWER	923.2	332.9	64.0
	WEB 2	888.8	254.8	71.0
	UPPER 2	906.3	195.8	78.0
90	LOWER	994.4	447.9	55.0
	WEB 2	966.9	332.9	66.0
	UPPER 2	979.3	269.5	72.0
120	LOWER	1039.7	538.0	48.0
	WEB 2	1018.7	411.0	60.0
	UPPER 2	1025.9	348.1	66.0

Table 11 presents the proposed "b_i" coefficients used to determine the temperature in steel deck components when dealing with the composite slab with steel shield, maintaining their use in Equation (5). It is noted that in the lower region, the "b_2" parameters are small, since the rib is not protected, making the geometric parameters less relevant to the fire resistance.

Table 12 presents the proposed "b_i" coefficients for determining the temperature in steel deck components when dealing with the composite slab with the cavity protected by mineral wool, maintaining their use in Equation (5). The coefficient "b_1" is still big in comparison to the other coefficients, due to the insulation effect in the L3T regions.

Table 11. New coefficients "b_i" proposed to determine the temperature in steel deck under ISO 834 fire curve for a steel shield insulation.

TIME (min)	STEEL DECK REGION	b_0 (°C)	b_1 (°C.mm)	b_2 (°C.mm)	b_3 (°C)	b_4 (°C)
60	UPPER 2	655.63	−734.815	−0.32	193.9096	−52.90
	WEB 2	898.73	−18,071.9	−1.57	276.0602	−210.84
	LOWER	953.79	−868.995	−0.13	17.31293	−40.132
90	UPPER 2	770.62	−17,598.3	−1.14	511.3276	−186.22
	WEB 2	892.69	−12,026.7	−1.09	491.0991	−404.97
	LOWER	1047.78	−473.694	−0.09	7.664627	−57.90
120	UPPER 2	897.64	−16,998.5	−1.20	443.8899	−178.63
	WEB 2	973. 99	−5684.49	−0.61	228.0133	−188.25
	LOWER	980.55	−170.244	−0.05	75.57389	−14.705

Table 12. New coefficients "b_i" proposed to determine the temperature in steel deck under ISO 834 fire curve for a mineral wool insulation.

TIME (min)	STEEL DECK REGION	b_0 (°C)	b_1 (°C.mm)	b_2 (°C.mm)	b_3 (°C)	b_4 (°C)
60	UPPER 2	0	−80,115.3	−5.54224	1182.233	−0.00016
	WEB 2	546.542	−5772.11	−4.82394	291.80	−0.00262
	LOWER	953.796	−868.995	−0.13103	17.31	−40.1328
90	UPPER 2	0	−131,140	−8.22638	1844.938	−0.00041
	WEB 2	474.912	−0.3311	−4.53379	718.85	−378.888
	LOWER	1047.79	−473.694	−0.09809	7.66	−57.907
120	UPPER 2	0	−189,471	−11.2556	2582.478	0
	WEB 2	802.465	−13,254.1	−5.70221	325.1772	−0.00084
	LOWER	980.556	−170.244	−0.05367	75.57389	−14.7057

For the regions UPPER 1 and WEB 1, which are areas without any insulation, the calculations can be performed using the coefficients presented in the new approach proposed by Carlos Balsa et al. [45].

Tables 13 and 14 present new coefficients to determine the average temperatures of the rebars for the case of composite slabs with steel shield and cavity insulation using mineral wool, respectively, maintaining their use in Equation (6).

Table 13. New coefficients "c_i" are proposed to determine the temperature in steel deck under ISO 834 fire curve for a steel shield insulation.

TIME (min)	c_0 (°C)	c_1 (°C)	c_2 (°C.mm$^{0.5}$)	c_3 (°C.mm)	c_4 (°C/°)	c_5 (°C.mm)
60	947.1	−201.6	−268.1	−3.25	4.17	−4585.2
90	1027.5	−198.8	−176.1	−3.98	3.63	−14,491.4
120	1153.7	−271.6	−158.3	−3.92	2.94	−12,363.0

Table 14. New coefficients "ci" proposed to determine the temperature in steel deck under ISO 834 fire curve for a mineral wool insulation.

TIME (min)	c_0 (°C)	c_1 (°C)	c_2 (°C.mm$^{0.5}$)	c_3 (°C.mm)	c_4 (°C/°)	c_5 (°C.mm)
60	930.078	−292.355	−117.716	−3.74446	0.936562	−7273.17
90	963.447	−143.803	−177.807	−1.52391	1.434412	−10.1888
120	1007.2	−253.709	−198.434	−3.50322	4.105537	−8.06392

For the case of composite slabs with mineral wool plates (70 kg/m^3), the calculation of the temperature at the steel deck components includes two additional factors, which depend on the thickness of the insulating material. The governing Equation (13) for this insulation approach employs the coefficient "b_i" from Table 11, corresponding to steel shield insulation, and includes the parameters "b_5" and "b_6"; see Table 15.

$$\theta_a = b_0 + b_1\frac{1}{L_3} + b_2\frac{A}{L_r} + b_3\varnothing + b_4\varnothing^2 + b_5 * hi^{\frac{1}{h2^2}} + b_6\log\left(\frac{hi}{1}\right) \quad (13)$$

Table 15. New coefficients "b_i" proposed to determine the temperature in steel deck under ISO 834 fire curve for a mineral wool plate insulation.

TIME (min)	STEEL DECK REGION	b_5 (°C)	b_6 (°C)
60	Upper 1–2	81.8	−437.8
	Web 1–2	205.1	−518.687
	Lower	270.8	−580.242
90	Upper 1–2	261.2041	−598.867
	Web 1–2	295.8592	−605.429
	Lower	336.9763	−596.251
120	Upper 1–2	337.2489	−646.264
	Web 1–2	357.831	−641.31
	Lower	353.4428	−572.978

Equation (14) provides the temperature for the steel rebar component when dealing with composite slabs using mineral wool plates, where the coefficients "c_0" to "c_5" are obtained from Table 13. The new coefficient "c_6" is presented in Table 16.

$$\theta_s = c_0 + c_1\frac{u_3}{h_2} + c_2 z + c_3\frac{A}{L_r} + c_4\alpha + c_5\frac{1}{L_3} + c_6\log\left(\frac{hi}{1}\right) \quad (14)$$

Table 16. New coefficient "c_6" proposed to determine the temperature in rebars under ISO 834 fire curve for a mineral wool plate insulation.

TIME (min)	c_6 (°C)
60	930.078
90	963.447
120	1007.2

5.4. Load-Bearing Capacity Time (R)

To determine the load-bearing capacity of the slab ($M_{Rd,fi,t}$) under fire, the method presented in prEN1994-1-2 [24] involves using the temperatures defined by Equations (5) and (6) to determine the temperature of the steel deck elements and the rebar components, respectively. With the defined temperatures, the method requires the determination of the reduction factors for the yield stress (k_y) according to prEN 1994-1-2. The method neglects the effect of temperature on concrete. The first step is to define the neutral axis using Equation (15), where "A_i" represents the effective area of the steel stress zone, adjusted by the factor (k_y); "A_j" is the effective area of concrete resisting to compression; and "α" is the coefficient weighting the contribution of the tension zone, taken as 0.85. Once the neutral axis is established as a function of temperature, the second step is to determine

the load-bearing capacity of the structure using Equation (16), using the distance from the plastic neutral axis to the centroid of the elemental area (z_i and z_j).

$$\sum_{i=1}^{m} A_i k_{y,i}\left(\frac{f_{y,i}}{\gamma_{M,y}}\right) + \alpha_{slab}\sum_{j=1}^{n} A_j k_{c,j}\left(\frac{f_{c,j}}{\gamma_{M,c}}\right) = 0 \quad (15)$$

$$M_{Rd,fi,t} = \sum_{i=1}^{m} A_i z_i k_{y,i}\left(\frac{f_{y,i}}{\gamma_{M,y}}\right) + \alpha_{slab}\sum_{j=1}^{n} A_j z_j k_{c,j}\left(\frac{f_{c,j}}{\gamma_{M,c}}\right) \quad (16)$$

The graphs presented in Figure 12 demonstrate that the implementation of insulation systems, whether through steel shielding or the application of mineral wool, delays the heating of critical elements, particularly with mineral wool, which maintains higher load-bearing capacity ($M_{Rd,fi,t}$) for extended periods compared to the composite slab without insulation. This approach, compatible with prEN1994-1-2 [24], effectively integrates thermal and mechanical effects, offering a robust tool for designing and assessing structural fire resistance and addressing the gap regarding the lack of design methods for composite slabs with special ribs and insulation methods.

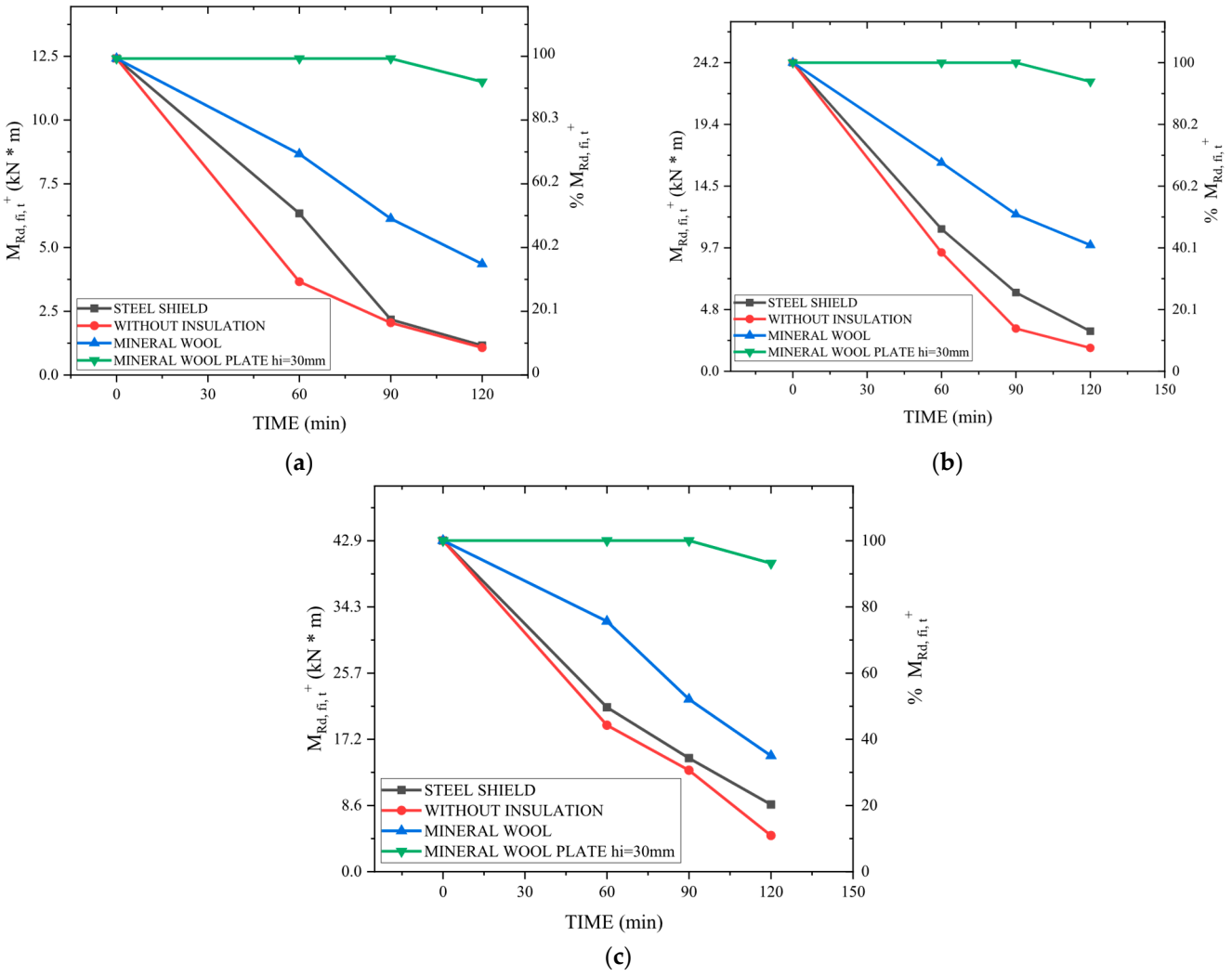

Figure 12. Evolution of the loss of load-bearing capacity of the slab ($M_{Rd,fi,t}$) over time under the ISO 834 fire curve for three conditions: without insulation, with a steel shield, and with mineral wool insulation. (**a**) VP50; (**b**) VP115; (**c**) VP200.

The mechanical analysis shows the fire resistance effect of different insulation strategies to leverage composite slabs' gain in mechanical strength under fire exposure, optimising and reducing concrete usage for sustainability purposes.

Conventional concrete emits approximately 430 kg/m^3 of CO_2 [46]. A reduction in concrete volume may be achieved by replacing a composite slab made with VP 200 (without insulation) with a VP 115 slab with 30 mm thick mineral wool board insulation (hi = 30 mm) to ensure 60 min fire resistance.

Table 17 presents a comparison of CO_2 emissions and the mechanical strength enhancement for slabs with 30 mm mineral wool board insulation and composite slabs without insulation. The carbon footprint per square metre of slab is calculated by summing the CO_2 emissions from the concrete and mineral wool. The mineral wool insulation (hi = 30 mm) has a CO_2 emission of 3.09 kg/m^2 [47].

Table 17. Carbon emissions in comparison to the load-bearing of the steel deck slabs.

STEEL DECK PLATE	Model Without Insulation		Mineral Wool Plate hi = 30 mm	
	Emissions of CO_2 (Kg/m^2)	Load-Bearing After 60 min (KN * m)	Emissions of CO_2 (Kg/m^2)	Load-Bearing After 60 min (KN * m)
VP 50	34.76	3.65	37.85	12.41
VP 115	42.40	9.34	45.49	24.27
VP 200	58.21	21.31	61.30	42.93

In the case of replacing VP 200 composite slabs with VP 115 composite slabs, including insulation, a reduction of approximately 20% in CO_2 emissions is achieved. This represents a significant figure, particularly in light of current demands for CO_2 reduction, given that cement is not only the most widely used material globally but also the largest contributor to CO_2 emissions within the construction sector.

6. Conclusions

This investigation presents an integrated and robust approach for assessing the thermal and mechanical behaviour of composite slabs with steel decks subjected to fire conditions, applying validated finite element models using ANSYS. One of the main objectives was to enhance the prediction of temperatures in critical components, such as the steel deck parts and reinforcement, through the calibration of new empirical coefficients ("a_i", "b_i", and "c_i") used in the simplified methods proposed by prEN1994-1-2, including the effect of a new stiffened steel deck and the use of insulation materials.

Specifically, the numerical modelling was divided into five stages: (i) Model validation was performed using experimental results from Fourie [21] and from Duponchel (CSTB) [27], which yielded a mean difference (RMS) of only 10.47 °C in the unexposed zone, despite larger deviations in regions such as WEB 2 (RMS ≈ 82.1 °C). (ii) Thermal analyses were implemented using PLANE55, LINK31, and LINK34 elements to accurately capture the temperature field in all the composite slabs using different insulation methods. (iii) A parametric study was conducted that compared the effectiveness of two insulation systems—the steel shield and mineral wool—revealing that, while the steel shield achieved a time gain of approximately 25% for the maximum temperature criterion. The mineral wool demonstrated a more pronounced effect by reducing temperatures in the upper zone (UPPER 2) by up to 89% compared to the uninsulated condition. (iv) The empirical coefficients were calibrated using a non-linear solver in Excel, which minimised the absolute difference between the simplified values and numerical results. (v) Strategies

were proposed for mitigating CO_2 emissions by utilising thermal insulation materials within composite slabs. Some strategies can reduce CO_2 emissions by more than 15 kg/m^2, enabling a spectrum of potential design configurations. This conclusion, however, is conditional on the specific geometries and materials of the parametric study, which revealed that while mineral wool above the steel shield can exceed standard requirements (EN13501-2), a 30 mm thickness may be insufficient for the highest fire resistance class (I240).

The results not only validate the effectiveness of the numerical model but also demonstrate that the introduction of insulation systems significantly enhances thermal integrity and, consequently, the load-bearing capacity of the slabs during fire events. The proposed methodology allows for a more accurate prediction of the fire resistance time, thereby enabling safer design of composite slabs in complex high-rise buildings. The choice of a constant air gap of 0.5 mm, addressing the debonding effect between the concrete and the steel, proved to be adequate, as already demonstrated by Piloto et al. [23].

Among the three insulation strategies evaluated, the mineral wool plate applied below the steel deck proved to be the most effective in enhancing both thermal insulation (I) and load-bearing capacity (R). It reduced temperatures in critical zones by up to 89% and increased fire resistance time proportionally with thickness, outperforming both the steel shield and cavity-filled mineral wool. The steel shield, while beneficial, offered the least improvement, with an estimated 25% gain in fire resistance time. These findings are consistently supported across all slab geometries (VP50, VP115, VP200) and insulation configurations tested, confirming the superior performance of mineral wool plates for fire-safe and sustainable composite slab design.

Finally, the development of new empirical coefficients and the validation of the simplified method represent a significant contribution to the field of structural fire safety. The proposed model coherently integrates thermal and mechanical effects, providing a robust tool for improving design and analysis methods for structures exposed to fire. Future studies may extend this approach by incorporating sensitivity analyses and additional experimental investigations to refine the adopted assumptions further, ultimately contributing to developing more precise and reliable design standards and guidelines.

7. Limitations and Future Works

This study identifies several limitations requiring further investigation. The practical applicability of the proposed insulation systems—encompassing constructability, durability, cost-effectiveness, adhesive performance at elevated temperatures, and seismic resilience—requires real-world verification. Model assumptions, such as a constant air gap for debonding and the neglect of thermal contact resistance at interfaces, alongside validation discrepancies (e.g., RMS up to 82.1 °C), indicate a need for enhanced thermal modelling, including dynamic gap evolution and three-dimensional effects (e.g., edge radiation, load redistribution). Critical structural aspects overlooked include shear failure mechanisms, particularly at rib roots, and the exclusion of cooling-phase effects where insulation may exacerbate thermal gradients, residual stresses, and delayed failures. Analyses were also limited to the ISO 834 standard fire, neglecting natural fire scenarios involving compartment interactions, moisture effects, and cooling-phase behaviour.

Future research should focus on developing 3D thermo-mechanical models incorporating dynamic air gaps and shear failure criteria (e.g., EN 1992-1-2); quantifying cooling-phase impacts on structural recovery; validating findings through full-scale testing across varied geometries and insulation types; and testing insulation robustness under cyclic thermal exposure, including bonded mineral wool plates and alternative materials (e.g., gypsum boards) or hybrid solutions. Investigating natural fires with compartment interactions and moisture content, alongside establishing design guidelines for fire-induced displace-

ments of steel shields, is essential to enhance the safety and sustainability of fire-resistant composite slabs.

Author Contributions: Conceptualization, P.A.G.P.; methodology, P.A.G.P. and O.G.N.R.; software, P.A.G.P. and O.G.N.R.; validation, O.G.N.R.; formal analysis, P.A.G.P. and O.G.N.R.; investigation, O.G.N.R.; resources, P.A.G.P.; data curation, O.G.N.R.; writing—original draft preparation, P.A.G.P., O.G.N.R. and G.d.M.S.G.; writing—review and editing, P.A.G.P., O.G.N.R. and G.d.M.S.G.; visualization, O.G.N.R.; supervision, P.A.G.P. and G.d.M.S.G.; project administration, P.A.G.P. All authors have read and agreed to the published version of the manuscript.

Funding: This research received no external funding.

Conflicts of Interest: The authors declare no conflict of interest.

References

1. Filho, M.M.A.; Piloto, P.A.G.; Balsa, C. Thermal behaviour of rebars and steel deck components of composite slabs under natural fire. *J. Compos. Sci.* **2022**, *6*, 232. [CrossRef]
2. Yu, X.; Huang, Z.; Burgess, I.; Plank, R. Non-linear analysis of orthotropic composite slabs in fire. *Eng. Struct.* **2008**, *30*, 67–80. [CrossRef]
3. Pantousa, D.; Mistakidis, E. Advanced modeling of composite slabs with thin-walled steel sheeting submitted to fire. *Fire Technol.* **2013**, *49*, 293–327. [CrossRef]
4. Centers for Disease Control and Prevention. Deaths resulting from residential fires and the prevalence of smoke alarms--United States, 1991–1995. *MMWR Morb. Mortal. Wkly. Rep.* **1998**, *47*, 803–806.
5. Cowlard, A.; Bittern, A.; Abecassis-Empis, C.; Torero, J. Fire safety design for tall buildings. *Procedia Eng.* **2013**, *62*, 169–181. [CrossRef]
6. Ma, J.; Song, W.G.; Tian, W.; Lo, S.M.; Liao, G. Experimental study on an ultra high-rise building evacuation in China. *Saf. Sci.* **2012**, *50*, 1665–1674. [CrossRef]
7. Holborn, P.G.; Nolan, P.F.; Golt, J. An analysis of fatal unintentional dwelling fires investigated by London Fire Brigade between 1996 and 2000. *Fire Saf. J.* **2003**, *38*, 1–42. [CrossRef]
8. Kobes, M.; Helsloot, I.; de Vries, B.; Post, J.G. Building safety and human behaviour in fire: A literature review. *Fire Saf. J.* **2010**, *45*, 1–11. [CrossRef]
9. Zhang, X. Study on rapid evacuation in high-rise buildings. *Eng. Sci. Technol. Int. J.* **2017**, *20*, 1203–1210. [CrossRef]
10. Buchanan, A.H.; Abu, A.K. *Structural Design for Fire Safety*; John Wiley & Sons: Hoboken, NJ, USA, 2017.
11. Gillie, M.; Usmani, A.; Rotter, M.; O' Connor, M. Modelling of heated composite floor slabs with reference to the Cardington experiments. *Fire Saf. J.* **2001**, *36*, 745–767. [CrossRef]
12. Jiang, J.; Cai, W.; Chen, W.; Ye, J.; Li, G.-Q. An insight into eurocode 4 design rules for thermal behaviour of composite slabs. *Fire Saf. J.* **2021**, *120*, 103084. [CrossRef]
13. *ISO 834-1*; Fire Resistance Tests—Elements of Building Construction—Part 1: General Requirements. International Organization for Standardization: Geneva, Switzerland, 1999.
14. Chau, C.K.; Hui, W.K.; Ng, W.Y.; Powell, G. Assessment of CO_2 emissions reduction in high-rise concrete office buildings using different material use options, Resour. *Conserv. Recycl.* **2012**, *61*, 2234. [CrossRef]
15. Azarbayjani, M.; Thaddeus, D.J. Environmental Dimensions of Climate Change: Endurance and Change in Material Culture. In *Towards Net Zero Carbon Emissions in the Building Industry*; Springer International Publishing: Cham, Switzerland, 2022; pp. 293–371. [CrossRef]
16. British Steel. *The Behaviour of Multi-Storey Steel Frame Buildings in Fire*; British Steel: Rotherham, UK, 1999.
17. Wald, F.; Da Silva, L.S.; Moore, D.B.; Lennon, T.; Chladna, M.; Santiago, A.; Beneš, M.; Borges, L. Experimental behaviour of a steel structure under natural fire. *Fire Saf. J.* **2006**, *41*, 509–522. [CrossRef]
18. Gernay, T.; Franssen, J.-M. A performance indicator for structures under natural fire. *Eng. Struct.* **2015**, *100*, 94–103. [CrossRef]
19. Ramesh, S.; Ramesh, S.; Choe, L.; Seif, M.; Hoehler, M.; Grosshandler, W.; Sauca, A.; Bundy, M.; Luecke, W.E.; Bao, Y.; et al. *Compartment Fire Experiments on Long-Span Composite-Beams with Simple Shear Connections Part 1*; NIST Technical Note 2054; US Department of Commerce, National Institute of Standards and Technology: Gaithersburg, MD, USA, 2019. [CrossRef]
20. Choe, L.Y.; Ramesh, S.; Hoehler, M.S.; Seif, M.S.; Bundy, M.F.; Reilly, J.; Glisic, B. *Compartment Fire Experiments on Long-Span Composite-Beams with Simple Shear Connections Part 2*; NIST Technical Note 2054; US Department of Commerce, National Institute of Standards and Technology: Gaithersburg, MD, USA, 2019. [CrossRef]

21. Fourie, S.J. Design and Construction of an Intermediate-Scale Fire Resistance Furnace, with Commissioning and Validation on a Novel Composite Floor System. Ph.D. Thesis, Stellenbosch University, Stellenbosch, South Africa, 2020.
22. Bennett, T.M.; Allan, J.F.; Garden, J.A.; Shaver, M.P. Low Formaldehyde Binders for Mineral Wool Insulation: A Review. *Glob. Chall.* **2022**, *6*, 2100110. [CrossRef]
23. Piloto, P.A.; Balsa, C.; Santos, L.M.; Kimura, É.F. Effect of the load level on the resistance of composite slabs with steel decking under fire conditions. *J. Fire Sci.* **2020**, *38*, 212–231. [CrossRef]
24. *prEN 1994-1-2*; Design of Composite Steel and Concrete Structures—Part 1–2: General Rules—Structural Fire Design. CEN—European Committee for Standardization: Brussels, Belgium, 2024.
25. Jiang, J.; Pintar, A.; Weigand, J.M.; Main, J.A.; Sadek, F. Improved calculation method for insulation-based fire resistance of composite slabs. *Fire Saf. J.* **2019**, *105*, 144–153. [CrossRef]
26. *ANSYS*®, Academic Research Mechanical, Release R2; ANSYS, Inc.: Canonsburg, PA, USA, 2024.
27. Duponchel, X. Etude du comportement au feu du plancher COFRADAL 200. Centre Scientifique et Technique du Bâtiment (CSTB), 21 Dec. 2006. Report no. 26004514, ArcelorMittal.
28. Claasen, J.; Cicione, A.; Streicher, D.; Walls, R. Behavior of a Composite Steel Decking and Boarding System in Fire Based on Large-Scale Experimental Testing and Numerical Modelling. *Fire Technol.* **2023**, *59*, 2389–2414. [CrossRef]
29. Thompson, M.K.; Thompson, J.M. *ANSYS Mechanical APDL for Finite Element Analysis*; Butterworth-Heinemann: Oxford, UK, 2017.
30. Balsa, C.; Silveira, M.; Mange, V.; Piloto, P.A.G. Modelling the Thermal Effects on Structural Components of Composite Slabs under Fire Conditions. *Computation* **2022**, *10*, 94. [CrossRef]
31. *EN-1991-1-2*; Eurocode 1: Actions on Structures—Part 1-2: General Actions—Actions on Structures Exposed to Fire. CEN—European Committee for Standardization: Brussels, Belgium, 2002.
32. Khetata, S.M.; Piloto, P.A.; Gavilán, A.B. Fire resistance of composite non-load bearing light steel framing walls. *J. Fire Sci.* **2020**, *38*, 136–155. [CrossRef]
33. Torres, L.; Couto, C.; Real, P.V.; Piloto, P. Numerical study of the fire behaviour of external walls in light steel framing. *Fire Saf. J.* **2023**, *141*, 103946. [CrossRef]
34. Piloto, P.A.; Khetata, M.S.; Ramos-Gavilán, A.B. Analysis of the critical temperature on load bearing LSF walls under fire. *Eng. Struct.* **2022**, *270*, 114858. [CrossRef]
35. Çengel, Y.A.; Ghajar, A.J. *Heat and Mass Transfer: Fundamentals and Applications*, 6th ed.; McGraw-Hill Education: Columbus, OH, USA, 2020.
36. Voidcon Group. *Voidcon—Innovative Permanent Formwork*. 2025. Available online: https://www.clotansteel.co.za/portfolio-item/permanent-formwork-voidcon/ (accessed on 28 July 2025).
37. *FprEN 1993-1-2*; Eurocode 3: Design of Steel Structures—Part 1-2: General Rules—Structural Fire Design. CEN—European Committee for Standardization: Brussels, Belgium, 2023.
38. *prEN 1995-1-2*; Eurocode 5: Design of Timber Structures—Part 1-2: Structural Fire Design. CEN—European Committee for Standardization: Brussels, Belgium, 2023.
39. ROCTERM+. Rocterm PN 70: Painel de Lã de Rocha Não Revestido. Obras360, 2020. Available online: https://www.obras360.pt/0010010021-la-de-rocha-isolamento-termico-acustico-painel-nao-revestido-rocterm-pn-70-70-kg-m3 (accessed on 28 July 2025).
40. *ISO 1461*; Hot Dip Galvanized Coatings on Fabricated Iron and Steel Articles—Specifications and Test Methods. 4th ed. International Organization for Standardization: Geneva, Switzerland, 2022.
41. *ISO 14713-2*; I Zinc Coatings—Guidelines and Recommendations for the Protection Against Corrosion of Iron and Steel in Structures—Part 2: Hot Dip Galvanizing. 2nd ed. International Organization for Standardization: Geneva, Switzerland, 2019.
42. *EN 1363-1:2020*; Fire Resistance Tests—Part 1: General Requirements. CEN—European Committee for Standardization: Brussels, Belgium, 2020.
43. *EN 13501-2:2009*; Fire Classification of Construction Products and Building Elements—Part 2: Classification Using Data from Fire Resistance Tests, Excluding Ventilation Services. CEN—European Committee for Standardization: Brussels, Belgium, 2009.
44. Barati, R. Application of excel solver for parameter estimation of the non-linear Muskingum models. *KSCE J. Civ. Eng.* **2013**, *17*, 1139–1148. [CrossRef]
45. Balsa, C.; Ribeiro, F.; Piloto, P.A.G.; Rigobello, R. A new calculation method for the temperature of the components of composite slabs under fire. *J. Comput. Appl. Mech.* **2021**, *52*, 206–214. [CrossRef]

46. Zhao, Y.; Wang, T.; Yi, W. Emergy-accounting-based comparison of carbon emissions of solid waste recycled concrete. *Constr. Build. Mater.* **2023**, *387*, 131674. [CrossRef]
47. Huang, M.C.; Zhang, Y.J. Carbon emissions analysis of rock wool board products. In *Materials Science Forum*; Trans Tech Publications Ltd.: Baech, Switzerland, 2020; Volume 993. [CrossRef]